Canister Centerline Cooling Experiments for DPF5-336 Reference Material Made with ERV3b Salt Simulant

Nuclear Technology Research and Development

Prepared for U.S. Department of Energy Material Recovery and Waste Form Development Campaign

B.J. Riley, S. Chong, and E.T. Nienhuis
Pacific Northwest National Laboratory
February 3, 2023
PNNL-33802



DISCLAIMER

This information was prepared as an account of work sponsored by an agency of the U.S. Government. Neither the U.S. Government nor any agency thereof, nor any of their employees, makes any warranty, expressed or implied, or assumes any legal liability or responsibility for the accuracy, completeness, or usefulness, of any information, apparatus, product, or process disclosed, or represents that its use would not infringe privately owned rights. References herein to any specific commercial product, process, or service by trade name, trade mark, manufacturer, or otherwise, does not necessarily constitute or imply its endorsement, recommendation, or favoring by the U.S. Government or any agency thereof. The views and opinions of authors expressed herein do not necessarily state or reflect those of the U.S. Government or any agency thereof.

SUMMARY

This report provides experimental details and results on the elemental distributions (compositions), crystalline/amorphous phase distribution, and microstructures for DPF5-336 reference materials made with ERV3b salt that were subjected to the canister centerline cooling (CCC) heat treatment process. To fabricate these materials, ammonium dihydrogen phosphate was mixed with ERV3b salt simulant and a dechlorination procedure was run in the generation-2 dechlorinator at the Pacific Northwest National Laboratory up to 600°C in an alumina crucible. After the dechlorination process, the product was removed from the crucible, lightly crushed, loaded into a new alumina crucible, Fe₂O₃ was added, and this was vitrified at 1100°C for 1 hour and quenched. The quenched material was mostly amorphous but showed some small diffraction peaks attributed to Li₃Fe₂(PO₄)₃. This quenched material was ground to a fine particle size in a milling chamber, and this was subjected to the CCC cooling profile in duplicate within alumina and fused quartz crucibles. The CCC experiment is designed to simulate the slowest cooling profile (the vertical centerline) of a 0.61-m diameter canister where the slower cooling profile often results in the production of a variety of different crystalline phases upon formation of which result in a residual glass of unknown composition and properties. The information gleaned from these types of experiments will lead to improved composition-property predictions for materials with similar compositions. The results of the alumina and fused quartz experiments show different microstructures but similar diffraction patterns providing evidence of similar crystalline phases being present in each sample. Both samples had monazite [i.e., (Ce,Nd)PO₄] and mixtures of phases containing P, Fe, and alkali metal elements. This report completes the milestone M4FT-23PN030104042 with details provided in Appendix B.

CONTENTS

SUM	MARY	iii
ACR	ONYMS AND ABBREVIATIONS	ix
1.0	Introduction	1
2.0	Experimental Methods 2.1 Sample Production 2.2 Canister Centerline Cooling (CCC) Treatments 2.3 Sample Characterization	3
3.0	Results and Discussion	6
4.0	Summary and Conclusions	17
5.0	Acknowledgements	18
6.0	References	19
Appe	ndix A SEM-EDS Data	20
Appe	ndix B Milestone Details	25
	FIGURES	
Figur	te 1. Fe ₂ O ₃ -P ₂ O ₅ -salt ternary diagram (in mole fraction) showing the original six DPF compositions (DPF-1 – DPF-6) along with the phase-2 compositions of DPF-3 variations (with different Fe:P molar ratios and fixed salt) as well as DPF-5 variations (with fixed Fe:P ratios and different salt contents) synthesized starting from ERV2 salt simulant compositions (Ebert and Fortner 2019a, 2019b; Riley and Chong 2019; Riley et al. 2020; Stariha and Ebert 2020).	1
Figur	e 2. Generation-2 dechlorination apparatus at PNNL used for removing halides from ERV3b salt simulants prior to high-temperature vitrification documented in Riley et al. (2021)	
Figur	re 3. The canister centerline cooling (CCC) curve performed for the DPF5-336 (ERV3b) reference materials produced in this study.	5
Figur	te 4. Experimental setup used for running CCC heat treatments showing the double-crucible technique showing the (a) side view and (b) top view	6
Figur	re 5. Pictures of (a) the dechlorination product and (b) vitrified product of DPF5-336 materials (Riley and Chong 2022)	7
Figur	ce 6. XRD data for the quenched DPF5-336 reference materials made with ERV3b compositions including (top pattern; sample G1) after vitrification using oxides, carbonates, and ADP and (bottom pattern) the same composition made by dechlorinating ERV3b salt followed by vitrification; see Riley et al. (2023) for more	

	information. While both samples appear mostly amorphous, small peaks marked with red dots fit the ICDD pattern for Li ₃ Fe ₂ (PO ₄) ₃ (see inset plot shown with background subtracted).	8
Figure 7.	Pictures of DPF5-336 samples following CCC treatments in (a,c) a fused quartz crucible and (b,d) an alumina crucible including (a,b) cross-sectioned views in resin and (c,d) the samples prior to cross-sectioning while still in the original crucibles and secondary containment crucibles.	9
Figure 8.	XRD patterns showing the DPF5-336-CCC samples run in alumina and fused quartz crucibles. The peak locations and intensities are very similar. (c) A summary of possible peak fits from the International Centre for Diffraction Data (ICDD) for the alumina sample.	10
Figure 9.	Summary of possible peak fits from the ICDD for the alumina sample	10
Figure 10	SEM micrographs at (a,c,e) 80× and (b,d,f) 250× magnifications of the (a,b) top, (c,d) middle, and (e,f) bottom portion of the cross-sectional view of the sample CCC-treated in the fused quartz crucible (see Figure 7a,c). Cracks and void spaces are seen as dark black regions.	11
Figure 11	. SEM micrographs at (a,c,e) 80× and (b,d,f) 250× magnifications of the (a,b) top, (c,d) middle, and (e,f) bottom portion of the cross-sectional view of the sample CCC-treated in the alumina crucible (see Figure 7b,d). Cracks and void spaces are seen as dark black regions.	12
Figure 12	SEM-EDS dot map data for the CCC-treated sample run in the fused quartz crucible (see Figure 7a,c), which can be seen at the bottom of the map with an air gap between the sample and the crucible in Figure 10e,f, which is also the location in the sample where this map was collected.	13
Figure 13	. SEM-EDS dot map data for the CCC-treated sample run in the alumina crucible (see Figure 7b,d); the bottom of the sample is seen in the Al dot map where the crucible-sample interface can be observed. The location of this region is at the bottom of the samples (see Figure 11e,f).	14
Figure 14	crucible. This region was in the middle of the sample (see Figure 10d). (bottom) EDS spot analysis from regions shown in the top figure from regions that are light gray (spots 7-9), medium gray (spots 1-3), dark gray (spots 4-6), and monazite (spots 10-12). The full dataset is found in Table A1 in Appendix A.	15
Figure 15	. (top) SEM-EDS spot locations for the CCC-treated sample run in the alumina crucible. This region was at the top of the sample (see Figure 11b). (bottom) EDS spot analysis from regions shown in the top figure from regions that are light gray (spots 1-3), medium gray (spots 4-6), dark gray (spots 7-9), and monazite (spots 10-12) were the values are averages across the spots along with error bars representing standard deviations ($\pm 1\sigma$). The full dataset is found in Table A2 in Appendix A.	16
APPEND	DIX FIGURES:	
	1. SEM micrographs for G1 at (a) 100×, (b) 150×, and (c) 2000× magnifications. The shadow in (a) is an artifact from the backscattered electron (BSE) detector	23
Figure A2	2. SEM-EDS dot map for G1 including the SEM micrograph, EDS overlay, and the elemental maps for P, Fe, K, O, and Na.	23

Figure A3. SEM micrograph with EDS spot analysis regions for G1 at the top of the sample where the phase separation meets the bulk matrix phase with data presented in Table A3.	24
TABLES	
Table 1. Compositions of ERV2 (Riley et al. 2020) and ERV3b salt simulants (mass%, based on measured values from chemical analysis of the as-made salts). The ERV2 salt was made at Idaho National Laboratory (INL) and the ERV3b salt was made at Argonne National Laboratory (ANL).	2
Table 2. Summary of compositional properties and comparisons for DPF5 (Riley et al. 2020), DPF5-336 made with ERV2 salt (Riley et al. 2019; Riley and Chong 2020), and DPF5-336 made with ERV3b salt (<i>current work</i>). Different ratios are also provided for the reactants. Note that ADP denotes NH ₄ H ₂ PO ₄ (ammonium dihydrogen phosphate)	2
Table 3. Expected composition of DPF5-336 glass after oxide conversion (mass%) starting with ERV3b simulant.	3
Table 4. Summary of the CCC cooling profile including the time (t) in hours for each step, the adjusted time (t _{adj}) for the heat treatments in this study (following the ramp heating procedure to get to 1050°C), and the setpoint temperature.	4
Table 5. Summary of samples for CCC tests including the crucible sizes used in each experiment as well as sample masses used. The "change" value is the mass change between before and after the heat treatment and ID = identification.	5
Table 6. Summary of NH ₄ Cl solid condensates in different locations of the off-gas system including tare (before) mass (m_b), mass after experiment (m_b), and collected condensate mass (m_b) along with references to where these locations can be found in the schematic for the apparatus (see Figure 2).	7
APPENDIX TABLES:	
Table A1. Summary of EDS data (in atomic%) for CCC sample run in the fused quartz crucible where spectra 1-3 are the medium gray phase, spectra 4-6 are the dark gray phase, spectra 7-9 are the light gray phase, and spectra 10-12 are the monazite phase. Below each set of triplicates are average (ave) and standard deviation (SD; ±1σ) values for those datasets. The appearances of these locations in the sample along with the plotted data are found in Figure 14.	21
Table A2. Summary of EDS data (in atomic%) for CCC sample run in the alumina crucible where spectra 1-3 are the light gray phase, spectra 4-6 are the medium gray phase, spectra 7-9 are the dark gray phase, and spectra 10-12 are the monazite phase. Below each set of triplicates are average (ave) and standard deviation (SD; $\pm 1\sigma$) values for those datasets. The appearances of these locations in the sample along with the plotted data are found in Figure 15	22
Table A3. Summary of EDS spot analysis results (atomic%) from G1 (see Figure A3) including the homogeneous matrix phase (regions 1-5) and phase-separated phase (regions 6-10) as well as average (ave) and standard deviation (SD; $\pm 1\sigma$) data for like regions	24

ACRONYMS AND ABBREVIATIONS

ADP ammonium dihydrogen phosphate (NH₄H₂PO₄)

ANL Argonne National Laboratory
CCC canister centerline cooling

D diameter (crucible)

DPF dehalogenated phosphate waste form with Fe₂O₃

EDS energy dispersive X-ray spectroscopy
ERV2 electrorefiner salt simulant version 2
ERV3b electrorefiner salt simulant version 3b

FY fiscal year

H height (crucible)
HT heat treatment
ID identification

ICDD International Centre for Diffraction Data (database)

INL Idaho National Laboratory

NEUP Nuclear Energy University Partnership
PNNL Pacific Northwest National Laboratory

SEM scanning electron microscopy

WT wall thickness (crucible)

XRD X-ray diffraction

1.0 Introduction

The aim of this report is to provide documentation for experiments that were run to evaluate the effects of a slow-cooling heat treatment on the "reference iron phosphate waste form" material regarding microstructure and elemental distribution to different amorphous or crystalline phases. The reference material is referred to as the DPF5-336 composition based off previous work done at Pacific Northwest National Laboratory (PNNL) and Argonne National Laboratory (ANL) (Ebert 2022; Ebert and Fortner 2019a, 2019b; Riley and Chong 2020, 2022a; Riley et al. 2019, 2020, 2023; Stariha and Ebert 2020, 2021, 2022). The ternary diagram in Figure 1 shows where the DPF5-336 reference material (shown as 0.336) falls within compositional space of Fe₂O₃-P₂O₅-salt (in mole fractions). The slow-cooling profile utilized is based off the cooling profile at the centerline of a 0.61-m diameter canister and this process is referred to as canister centerline cooling (CCC) where the specific cooling profile details are provided later in the experimental section.

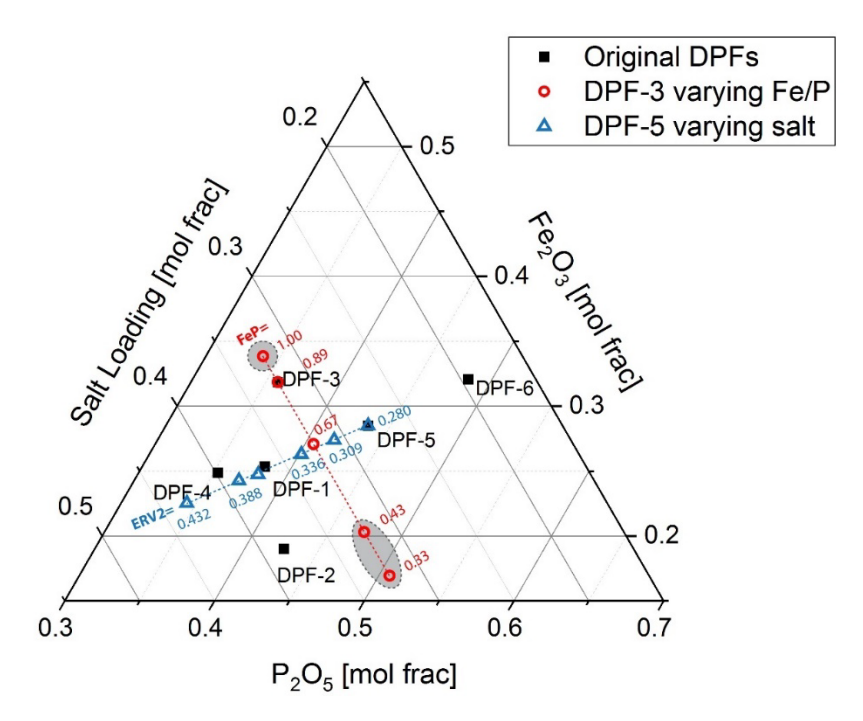


Figure 1. Fe₂O₃-P₂O₅-salt ternary diagram (in mole fraction) showing the original six DPF compositions (DPF-1 - DPF-6) along with the phase-2 compositions of DPF-3 variations (with different Fe:P molar ratios and fixed salt) as well as DPF-5 variations (with fixed Fe:P ratios and different salt contents) synthesized starting from ERV2 salt simulant compositions (Ebert and Fortner 2019a, 2019b; Riley and Chong 2019; Riley et al. 2020; Stariha and Ebert 2020).

It should be noted that, while previous studies utilized the ERV2 salt composition (Riley et al. 2020; Riley and Chong 2020), the new materials made utilize the ERV3b salt composition (see Table 1 for a comparison). The primary difference between ERV2 and ERV3b salt is the Cs constituent (CsI or CsCl) but other minor differences exist as well including different LiCl-KCl and NdCl₃ contents.

A compositional comparison between DPF5 (ERV2 salt), DPF5-336 (ERV2 salt), and DPF5-336 (ERV3b salt) is provided in Table 2. This comparison highlights the differences in the compositional parameters in terms of additive mass fractions and component (i.e., Fe, P, alkali, Cl, NH₄⁺) molar ratios but also highlights subtle differences in these ratios depending on the chosen salt simulant. The key differences between DPF5 and DPF5-336 are the higher salt content in DPF5-336 and thus the lower P:alkali and NH₄+:Cl molar ratios and higher Cl:P molar ratio. This difference in the NH₄⁺:Cl molar ratio results in less of a buffer (less excess NH₄⁺ to react with Cl) during the dechlorination process than what is achievable with the original DPF5 composition.

Table 1. Compositions of ERV2 (Riley et al. 2020) and ERV3b salt simulants (mass%, based on measured values from chemical analysis of the as-made salts). The ERV2 salt was made at Idaho National Laboratory (INL) and the ERV3b salt was made at Argonne National Laboratory (ANL).

Additive	ERV2	ERV3b
LiCl	32.32	32.05
KCl	38.68	39.06
NaCl	9.00	9.01
CsCl	ı	7.01
CsI	7.00	_
SrCl ₂	3.00	3.00
CeCl ₃	5.00	5.00
NdCl ₃	5.00	4.87

Table 2. Summary of compositional properties and comparisons for DPF5 (Riley et al. 2020), DPF5-336 made with ERV2 salt (Riley et al. 2019; Riley and Chong 2020), and DPF5-336 made with ERV3b salt (*current work*). Different ratios are also provided for the reactants. Note that ADP denotes NH₄H₂PO₄ (ammonium dihydrogen phosphate).

Comple	Salt	Compositions (mass%)			Ratios (molar basis)				
Sample	used	Salt	ADP	Fe ₂ O ₃	Fe:P	P:alkali	Cl:P	NH ₄ ⁺ :Cl	
DPF5	ERV2	20.00	55.00	25.00	0.655	1.64	0.667	1.50	
DPF5-336	ERV2	24.52	51.89	23.59	0.655	1.26	0.866	1.15	
DPF5-336	ERV3b	24.52	51.89	23.59	0.655	1.25	0.887	1.13	

In terms of comparisons, these three waste form materials were all fabricated differently as summarized here (see Table 1 for details on salt compositions and Table 2 for details on sample compositions):

- **DPF5** (*ERV2*). This sample was generated through dechlorination of ERV2 using the generation-1 dechlorination system. This work along with a description of the generation-1 dechlorination system is documented in Riley et al. (2020).
- **DPF5-336** (*ERV2*). This sample was synthesized starting from oxides and carbonates (no salt was used) whereby P and Fe were added using ammonium dihydrogen phosphate (ADP) and FePO₄. This work is documented in Riley et al. (2019).
- **DPF5-336** (*ERV3b*). This sample was synthesized starting from ERV3b salt received from ANL using the generation-2 dechlorination system. This work is described in the current document, but additional details about the generation-2 dechlorination system are provided in Riley et al. (2021).

For the CCC treatments, fused quartz and alumina crucibles were selected as containment vessels based on past CCC studies for DPF5 and the differences observed in the samples based on the crucible material selected (Riley and Chong 2022a; 2022b). It is unclear which crucible materials are best for the dechlorination process, vitrification process, and CCC-treatment process for DPF materials and this is one of the focuses of a Nuclear Energy University Partnership (NEUP) project starting in FY2023 in a joint

collaboration between PNNL, University of Nevada at Reno, Missouri University of Science and Technology, and University of Utah. At present, it is known that SiO₂ and Al₂O₃ are contaminants in the samples produced based on leaching from the crucibles into the melts (Riley et al. 2020; Riley and Chong 2020).

2.0 Experimental Methods

2.1 Sample Production

To produce the DPF5-336 (ERV3b) sample using the formulation shown in Table 2, 26.6003 g of ERV3b (simulant from ANL – see Table 1) and 56.2914 g of NH₄H₂PO₄ (>98.5%, Sigma Aldrich) were weighed on an analytical balance (ML304T00, Mettler Toledo) and added directly to a 250 mL alumina ceramic conical crucible (ACC3742; 99.8% purity; McDanel Advanced Ceramic Technologies). The filled crucible was loaded into the generation-2 dechlorination apparatus shown in Figure 2. The heat-treatment process utilized for the dechlorination procedure included ramp rates of 5°C/min with 10-min holds at 200°C, 300°C, and 400°C and a 1-hr hold at 600°C before allowing the furnace to cool to ambient temperature. The mass of NH₄Cl solid condensates collected in the off-gas glassware (see Figure 2b,c) were measured based on mass changes from before to after the heat treatment process for the off-gas capture glassware (see Figure 2b,c) and the solid condensates that fell into the crucible upon removal from the furnace and were recovered.

Following the dechlorination procedure, the cooled material was removed from the dechlorination furnace. The product in the crucible was mechanically removed by breaking the crucible with a hammer, it was lightly crushed, and 57.92 g (weighed on a Mettler Toledo PL1502E balance) of dechlorination product was added into a new 250 mL alumina crucible along with 29.9995 g of Fe₂O₃ (Baker Chemical Company) and mixed together. This filled crucible was loaded into a high-temperature Deltech furnace with a Pt/10%Rh lid. The mixture was vitrified by heating at 5°C/min to 1100°C, holding for 1 h at 1100°C, and then quenching the melt onto an Inconel® plate. The expected composition of the final DPF5-336 glass is shown in Table 3.

Table 3. Expected composition of DPF5-336 glass after oxide conversion (mass%) starting with ERV3b simulant.

Oxide	P_2O_5	Fe ₂ O ₃	Li ₂ O	K ₂ O	Na ₂ O	Cs ₂ O	SrO	CeO ₂	Nd ₂ O ₃
Mass%	46.28	34.10	4.00	8.75	1.69	2.08	0.70	1.24	1.16

Canister Centerline Cooling (CCC) Treatments 2.2

The DPF5-336 glass produced as described in Section 2.1 was ground to a powder in a tungsten carbide milling chamber, and the product from this grinding was the starting material for the subsequent heat treatments discussed below. The CCC heat treatments were performed on this quenched glass using a cooling profile used for Hanford high-level waste glasses used at the Hanford Waste Treatment and Immobilization Plant (WTP); a this cooling profile is shown in Table 4 with the temperature profile shown in Figure 3.

^a Memorandum, Canister Centerline Cooling Data, Revision 1, CCN: 074851, RPP-WTP, October 29, 2003.

Figure 2. Generation-2 dechlorination apparatus at PNNL used for removing halides from ERV3b salt simulants prior to high-temperature vitrification documented in Riley et al. (2021).

6.4-mm thick stainless steel

width: 38 cm

Table 4. Summary of the CCC cooling profile including the time (t) in hours for each step, the adjusted time (t_{adj}) for the heat treatments in this study (following the ramp heating procedure to get to 1050°C), and the setpoint temperature.

t	$t_{ m adj}$	T
hr	(hr, adj)	(°C)
0.00	3.47	1050
0.73	4.22	980
1.77	5.25	930
3.30	6.80	875
5.38	8.95	825
49.82	53.62	25

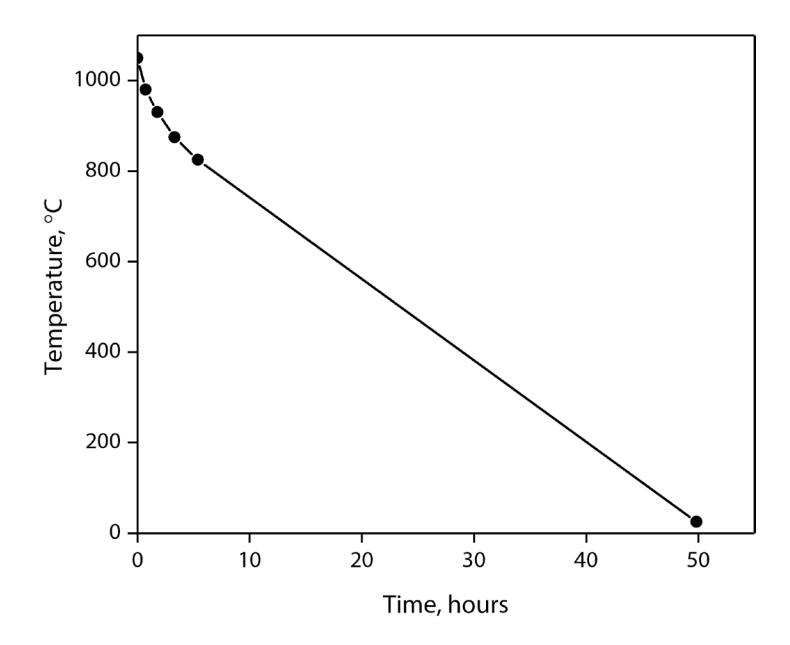


Figure 3. The canister centerline cooling (CCC) curve performed for the DPF5-336 (ERV3b) reference materials produced in this study.

To perform the CCC treatments, two sets of experiments were run where the crucibles used were either alumina (CoorsTek 65531, ~14.6-mm inner diameter, ~18.7-mm outer diameter, ~25-mm tall) or fused quartz (GE214, 17-mm inner diameter, 20-mm outer diameter, ~25-mm tall). In each case, the experiments were run in duplicate where equal amounts of ground DPF5-336 material were added to the two like crucibles. For the experiments run in alumina crucibles, ~4.5 g were added to each crucible and, for the fused quartz experiments, ~6.4 g were added where all crucibles were filled approximately to 75% of the total internal height of each crucible. For weighing out the DPF5-336 material, the ME204E balance was used.

Table 5. Summary of samples for CCC tests including the crucible sizes used in each experiment as well as sample masses used. The "change" value is the mass change between before and after the heat treatment and ID = identification.

Sample ID	Crucib	le size (m	nm) ^(a)	Sample mass, m (g) ^(b)			
Sample 1D	Н	D	WT	Before HT	After HT	Δm	
Alumina-1	26.64	18.59	2.1	4.4884	4.5108	+0.50%	
Alumina-2	26.82	18.80	2.0	4.6560	4.6779	+0.47%	
Quartz-1	28.02	20.02	1.5	6.3327	6.3651	+0.51%	
Quartz-2	27.45	20.02	1.5	6.5162	6.5486	+0.50%	

(a)H = height; D = outer diameter; WT = wall thickness; (b)HT = heat treatment, $\Delta m = [(After HT) - (Before HT)]/(Before HT).$

All filled crucibles were loaded into a secondary containment alumina crucible (ACN3764, 50 mL, McDanel Advanced Ceramic Technologies) to prevent ruining the furnace spill plate if material leaked out of the inner crucibles (see Figure 4). Alumina lids shown in Figure 4 were added to the secondary crucibles and each set was added to a box furnace to undergo the CCC treatment, described previously (see Table 4 and Figure 3). Based on thermocouple monitoring of this cooling curve in previously experiments (Riley and Chong 2020), the measured values were expected to fall very close to the desired cooling trend until the furnace cooling rate was limited by heat diffusion out of the furnace at T < 100°C. This temperature

deviation from the scheduled profile at T < 100°C was well below the glass transition temperature ($T_{\rm g}$) when the glass is a solid and does not impact the compositional and microstructural properties of these samples.

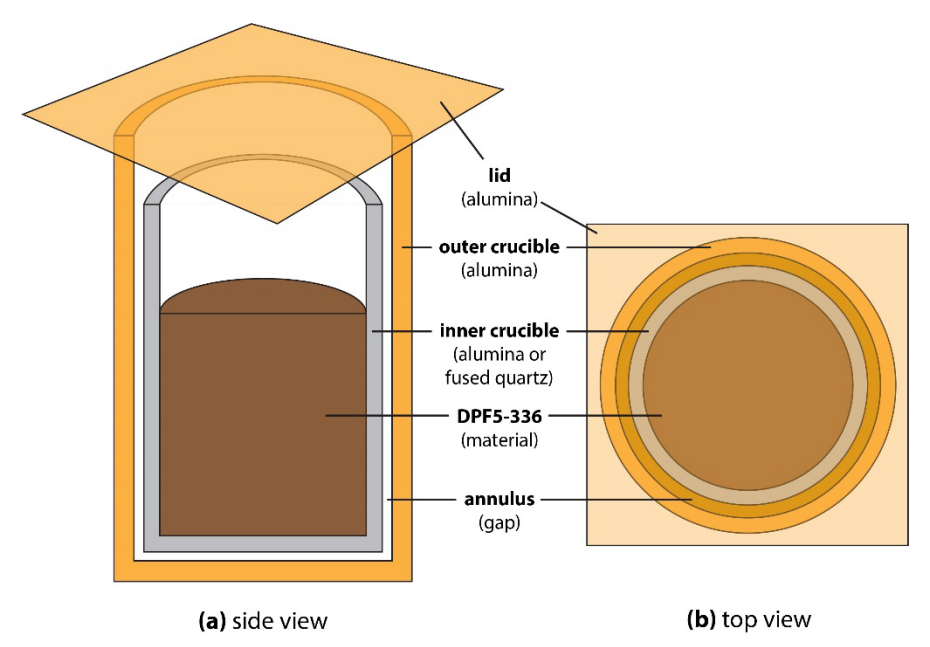


Figure 4. Experimental setup used for running CCC heat treatments showing the double-crucible technique showing the (a) side view and (b) top view.

Following the heat-treatment, the samples (in the inner crucibles – see Figure 4) were removed from the furnace, samples from each set (1 in an alumina crucible and 1 in a fused quartz crucible) were packaged and shipped to Argonne National Laboratory for chemical durability testing, and the other samples from each set were characterized at PNNL.

2.3 Sample Characterization

For the characterizations at PNNL, each sample was sectioned along the vertical axis using a variable speed saw with a diamond blade; the sectioning process resulted in two sample halves appearing similar to the image in Figure 4a (sample including the inner crucible only). Once each sample was cut vertically, once side of each sample was analyzed with X-ray diffraction (XRD) and the other half was mounted in resin, cut side down, for cross-sectional polishing. The XRD analysis was done on a crushed specimen upon removal from the inner crucible to prevent the artifact of the crucible material in the diffraction data. XRD data was collected on a Bruker D8 Advance diffractometer or a Rigaku SmartLab Studio II – both instruments contained Cu X-ray source. The polished specimen was then analyzed with scanning electron microscopy (SEM) and energy dispersive X-ray spectroscopy (EDS) using a JSM-7001F field emission gun SEM (JEOL USA) and an xFlash 6|60 EDS detector (Bruker AXS Inc.).

3.0 Results and Discussion

3.1 Dechlorination and Vitrification Process

The dechlorination process proceeded as expected based on five similar runs previously done on this same composition in fiscal year (FY) 2022 to provide the DPF5-336 reference material to ANL for chemical durability testing (Riley and Chong 2022). Pictures of both the dechlorination product and the final quenched DPF5-336 waste form are shown in Figure 5a and Figure 5b, respectively (Riley and Chong 2022). The dechlorination product was transparent and dark gray while the vitrified product was dark black

with a lustrous surface phase [attributed to Li₃Fe₂(PO₄)₃ – see Figure 6 and discussion below]. Based on the initial composition of the dechlorination batch and the ERV3b salt simulant used, the expected yield of NH₄Cl was 23.23 g and 21.38 g were captured (see Table 6). This recovered mass equates to a yield of 92.04 mass% and falls within the range of yields achieved for other batches reported by Riley and Chong (2022) of 84.54%–96.62%.

Table 6. Summary of NH₄Cl solid condensates in different locations of the off-gas system including tare (before) mass (m_b) , mass after experiment (m_b) , and collected condensate mass (m_b) along with references to where these locations can be found in the schematic for the apparatus (see Figure 2).

Location	Reference	$m_{\rm b}$ (g)	$m_{\rm a}$ (g)	$m_{\rm c}\left({\rm g}\right)$	Mass%
Тор	Figure 2c-1	153.29	163.68	10.39	48.59%
Middle	Figure 2c-2	134.28	144.19	9.91	46.35%
Bottom	Figure 2c-3	95.74	95.78	0.04	0.19%
Extension	Figure 2b	122.75	122.78	0.03	0.14%
Crucible	Figure 2f,d	_	_	1.013	4.74%
SUM	_	_	_	21.38	100.00%

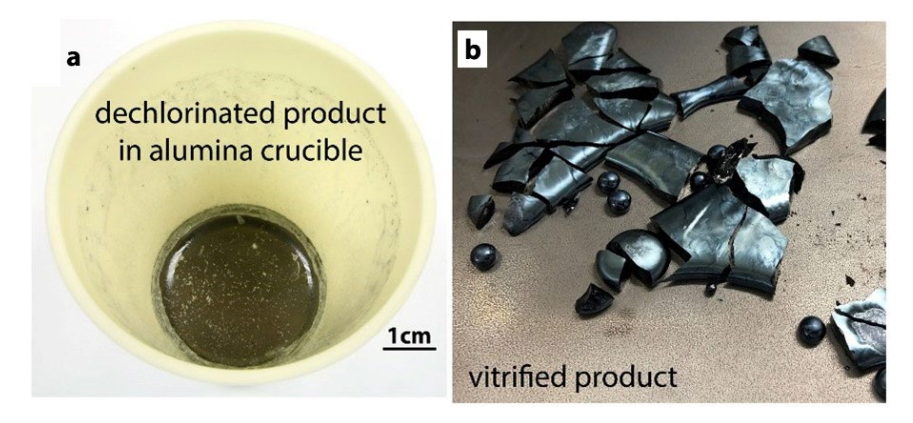


Figure 5. Pictures of (a) the dechlorination product and (b) vitrified product of DPF5-336 materials (Riley and Chong 2022).

The XRD data for the quenched DPF5-336 reference material is provided in Figure 6 (bottom scan) starting from ERV3b salt. In addition to this data the same material was also made during a different study where no salt was used but, rather, oxides and carbonates of the salt cations were reacted with ADP and Fe₂O₃ and this is the top scan in Figure 6 [sample G1 from Riley et al. (2023)]. Both patterns show broad amorphous diffraction peaks (humps) with some very small diffraction peaks that are attributed to a small quantity of crystalline material that fits well to the International Centre for Diffraction Data (ICDD) database pattern of Li₃Fe₂(PO₄)₃. The G1 sample after quenching was analyzed with cross-sectional SEM-EDS and showed some phase separation towards the top of the sample that cooled slowest during quenching; however, the compositional analysis shows that little variation could be found elementally between these different regions – see Appendix A (Section A-3; including Figure A1, Figure A2, Figure A3, and Table A3).

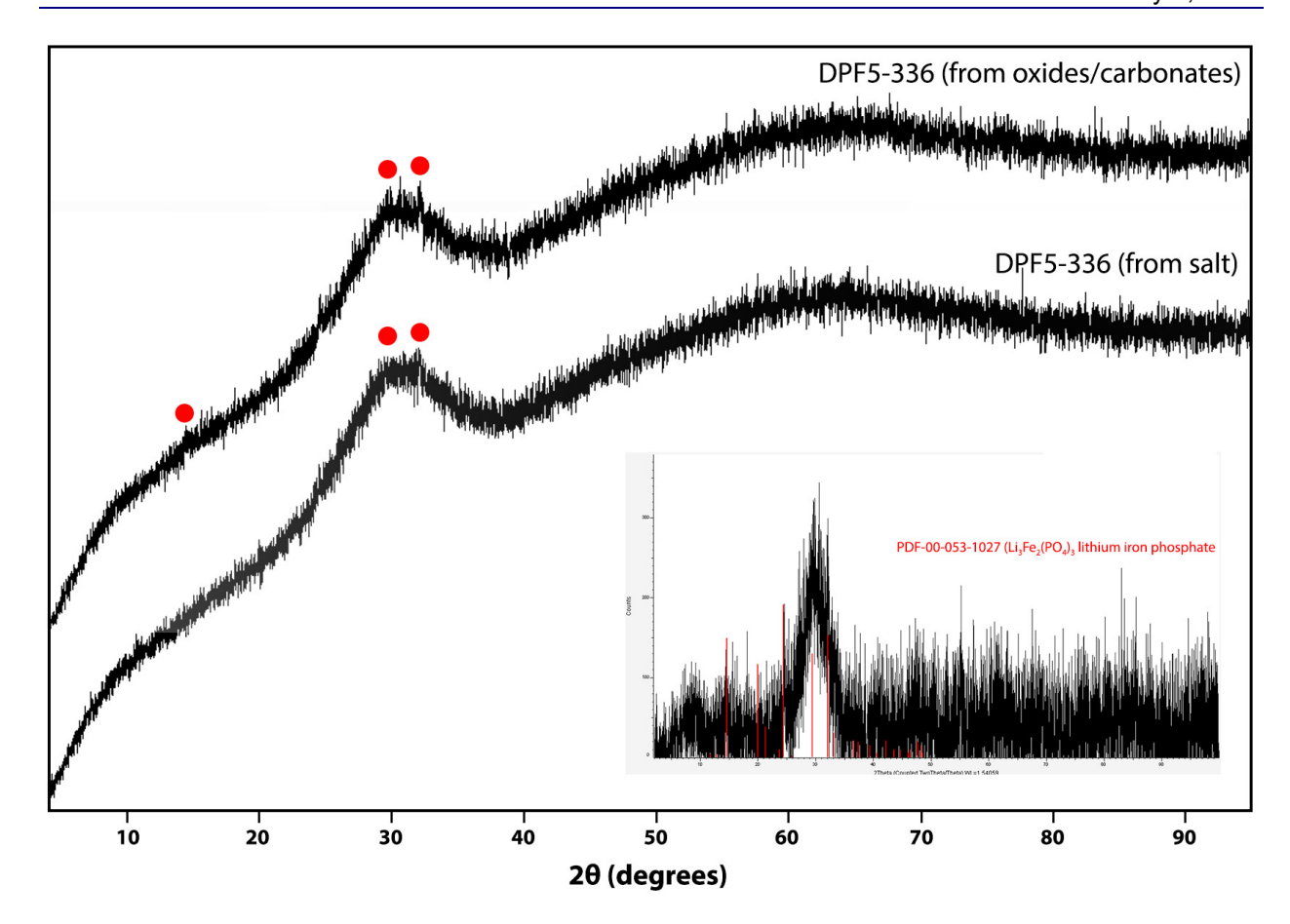


Figure 6. XRD data for the quenched DPF5-336 reference materials made with ERV3b compositions including (top pattern; sample G1) after vitrification using oxides, carbonates, and ADP and (bottom pattern) the same composition made by dechlorinating ERV3b salt followed by vitrification; see Riley et al. (2023) for more information. While both samples appear mostly amorphous, small peaks marked with red dots fit the ICDD pattern for Li₃Fe₂(PO₄)₃ (see inset plot shown with background subtracted).

3.2 CCC-Treated Samples

The cross-sections of the CCC-treated samples are shown in Figure 7a,b, which were captured using a flatbed scanner. Prior to the cross-section, images were captured of each sample while still in the secondary alumina containment crucibles and these images are shown in Figure 7c,d. Based on the images shown in Figure 7a,b, it is clear that the melt wetted the alumina crucible based on the dark color on the inner walls of the inner crucible and this was not the case with the fused quartz sample. Some discoloration was observed on the top rim of the fused quartz crucible as can be seen in Figure 7c but the top rim of the inner alumina crucible in Figure 7d was highly discolored by the melt. The cause for this difference between melt wettability of quartz versus alumina crucible walls is due to the porosity in the alumina and lack of porosity in the fused quartz. The cause of discoloration on the top rim of the fused quartz crucible is due to the fact that this was a ground surface and not a polished surface.

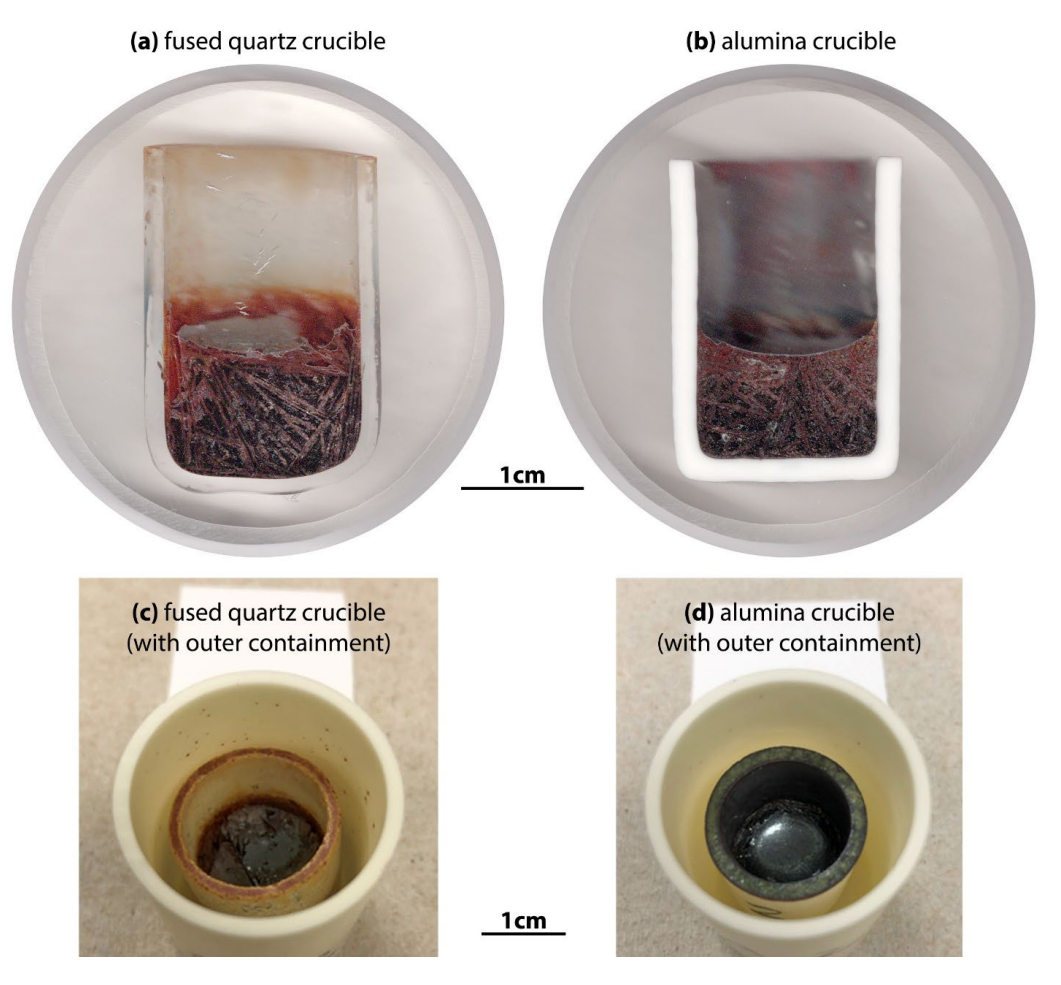


Figure 7. Pictures of DPF5-336 samples following CCC treatments in (a,c) a fused quartz crucible and (b,d) an alumina crucible including (a,b) cross-sectioned views in resin and (c,d) the samples prior to cross-sectioning while still in the original crucibles and secondary containment crucibles.

The XRD patterns for the samples run in the fused quartz crucible and the alumina crucible showed similar peak positions with some differences in peak intensities, indicating that both samples have similar crystalline phases (Figure 8). The major crystalline phase was Li₃Fe₂(PO₄)₃, and most of the identified phases were phosphates containing PO₄ or P₂O₇ in the structures based on peak location fitting with the ICDD database (Figure 9). However, due to different possible phase matches that were overlapping on the same 20 positions, it was difficult to accurately determine the crystalline phases. This shows how complicated the phase distribution is when CCC-treating iron phosphate waste forms and this complexity was also observed in similar studies previously with ERV2 salt on the DPF5 composition (Riley and Chong 2020).

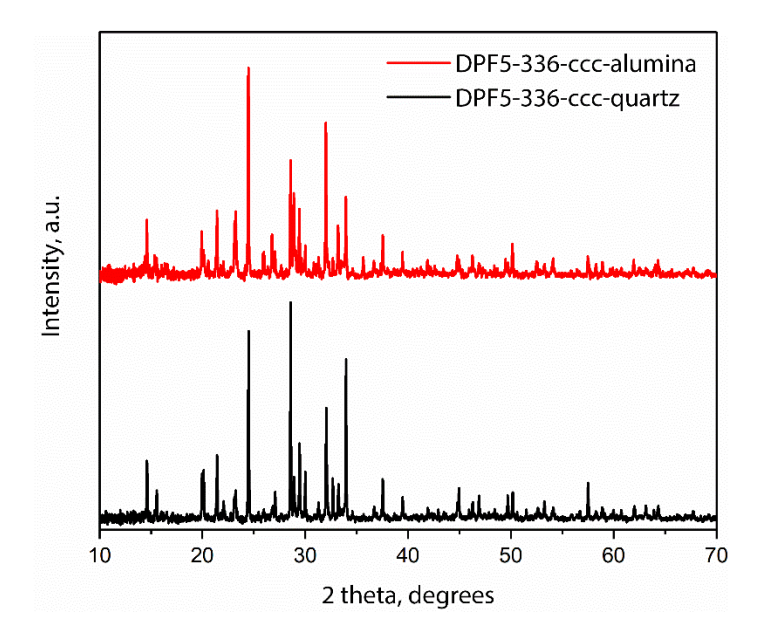


Figure 8. XRD patterns showing the DPF5-336-CCC samples run in alumina and fused quartz crucibles. The peak locations and intensities are very similar. (c) A summary of possible peak fits from the International Centre for Diffraction Data (ICDD) for the alumina sample.

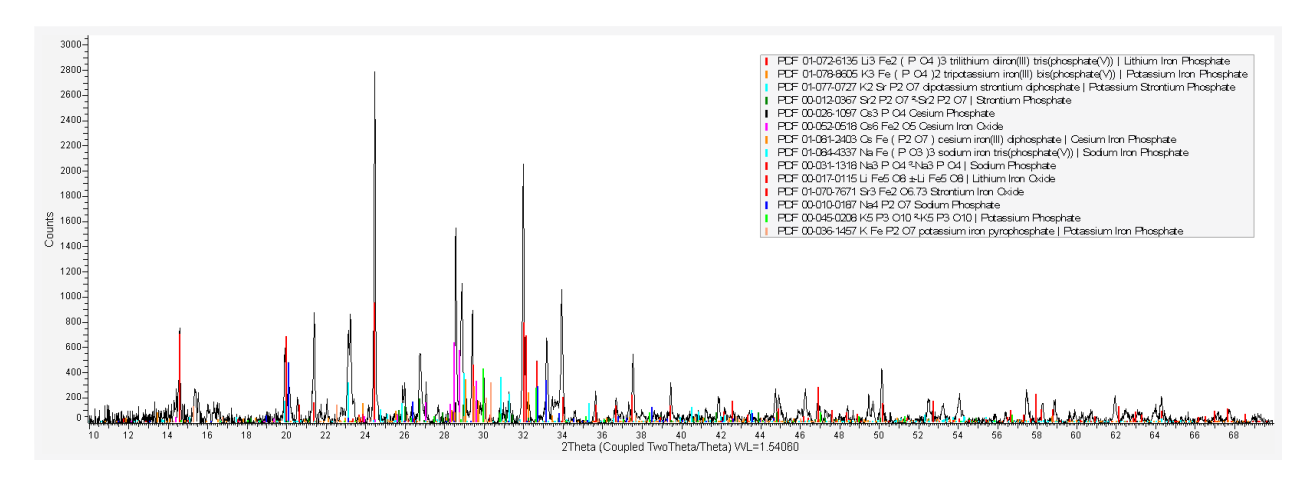


Figure 9. Summary of possible peak fits from the ICDD for the alumina sample.

Figure 10 and Figure 11 provide SEM micrograph collages of the CCC-treated material in the fused quartz and alumina crucibles, respectively. It should be noted that all of the EDS data exclude the quantification of Li based on limitations of the instrument and this analytical technique. These two sets of micrographs revealed some similarities as well as a few notable differences between the samples including the following:

- The microstructures were similar between both samples with darker/lighter matrix phases, some residual Fe₂O₃ phases, monazite (Ce,Nd)PO₄ phases, as well as some cracks and void spaces throughout. The monazite phases were seen interspersed, but with a large layer of crystals at the base of each sample (see Figure 10e,f and Figure 11e,f).
- The sample run in the alumina crucible had a lot of residual Fe₂O₃ present at the top of the sample as well as at the bottom of the sample in a thin layer. Also, small crystals of Fe₂O₃ were found dispersed along the bottom of the sample (see Figure 11a,b,e,f and Figure 13).

• The sample run in the alumina crucible was connected at the base to the crucible (Figure 11e,f)

whereas an air gap existed for the sample run in the fused quartz crucible (see Figure 10e,f).

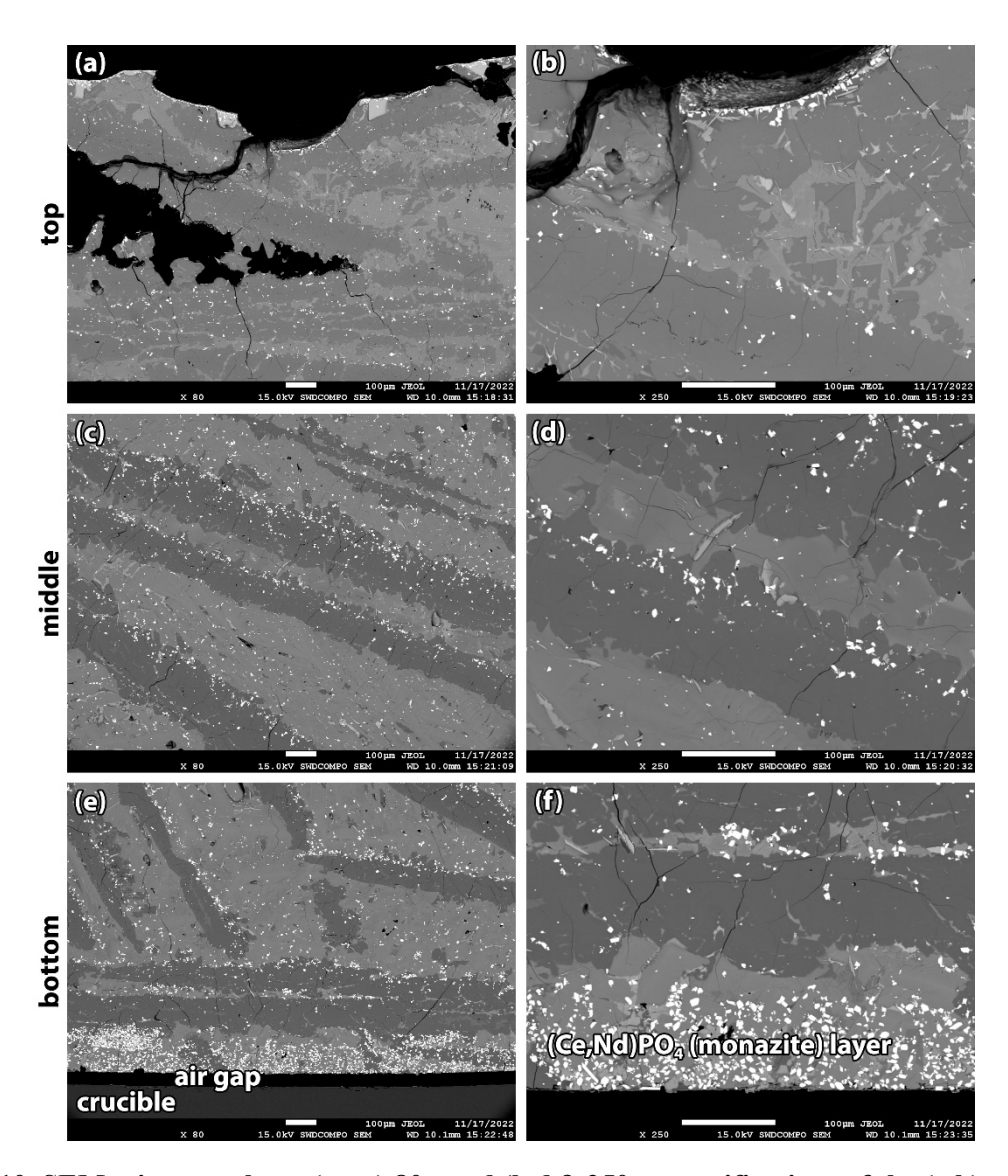


Figure 10. SEM micrographs at (a,c,e) 80× and (b,d,f) 250× magnifications of the (a,b) top, (c,d) middle, and (e,f) bottom portion of the cross-sectional view of the sample CCC-treated in the fused quartz crucible (see Figure 7a,c). Cracks and void spaces are seen as dark black regions.

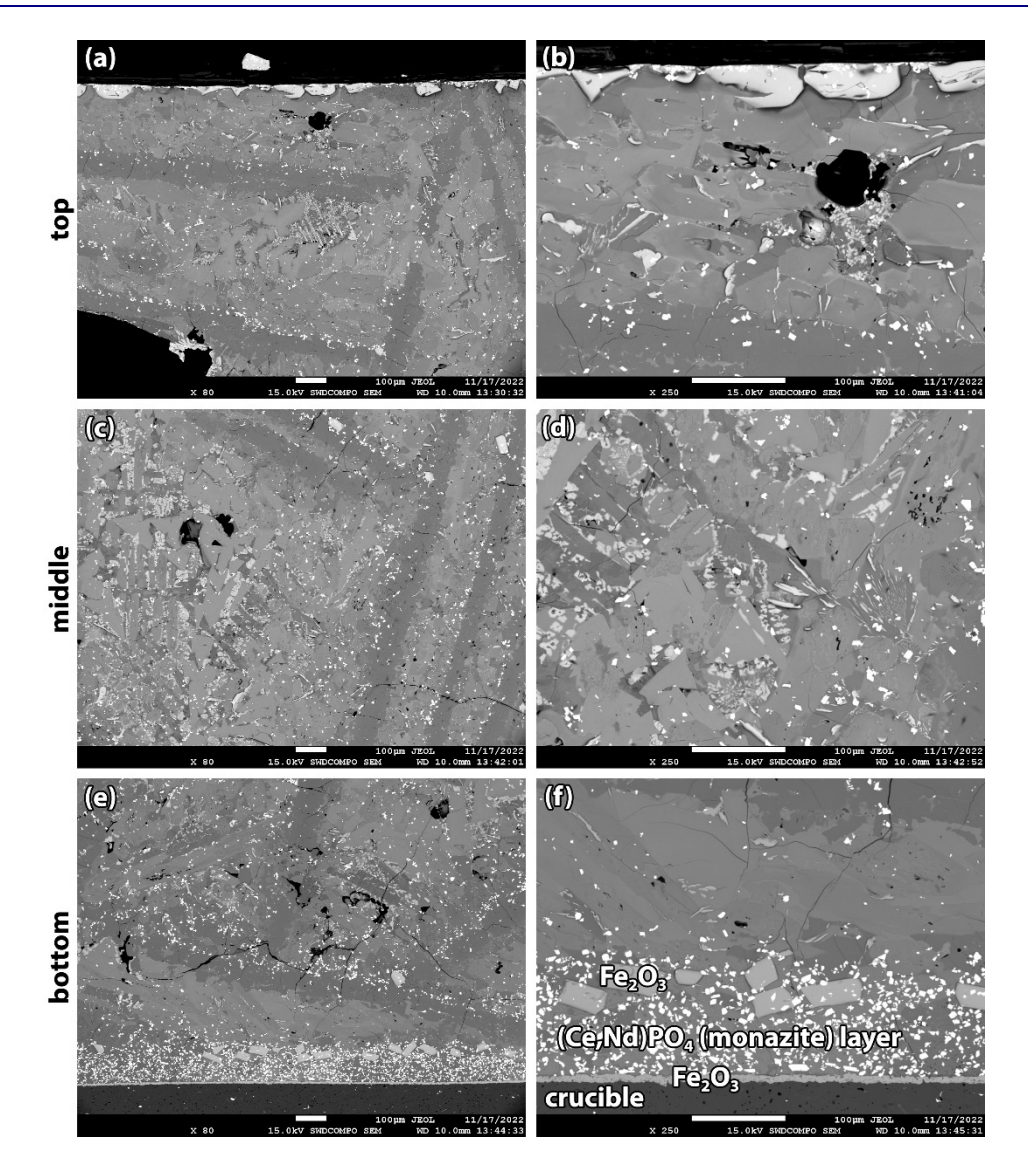


Figure 11. SEM micrographs at (a,c,e) 80× and (b,d,f) 250× magnifications of the (a,b) top, (c,d) middle, and (e,f) bottom portion of the cross-sectional view of the sample CCC-treated in the alumina crucible (see Figure 7b,d). Cracks and void spaces are seen as dark black regions.

The SEM-EDS dot maps for the CCC-treated samples run in fused quartz and alumina crucibles are shown in Figure 12 and Figure 13, respectively. Both of these EDS dot maps show variations in the elemental distributions between the different components from the dark matrix phase (P, Fe, Na) and light matrix phase (P, K, Cs, Al) to the monazite (Nd, Ce, P). Also, based on the K map specifically, it is clear that fluctuations exist between different phases that are likely very similar in composition.

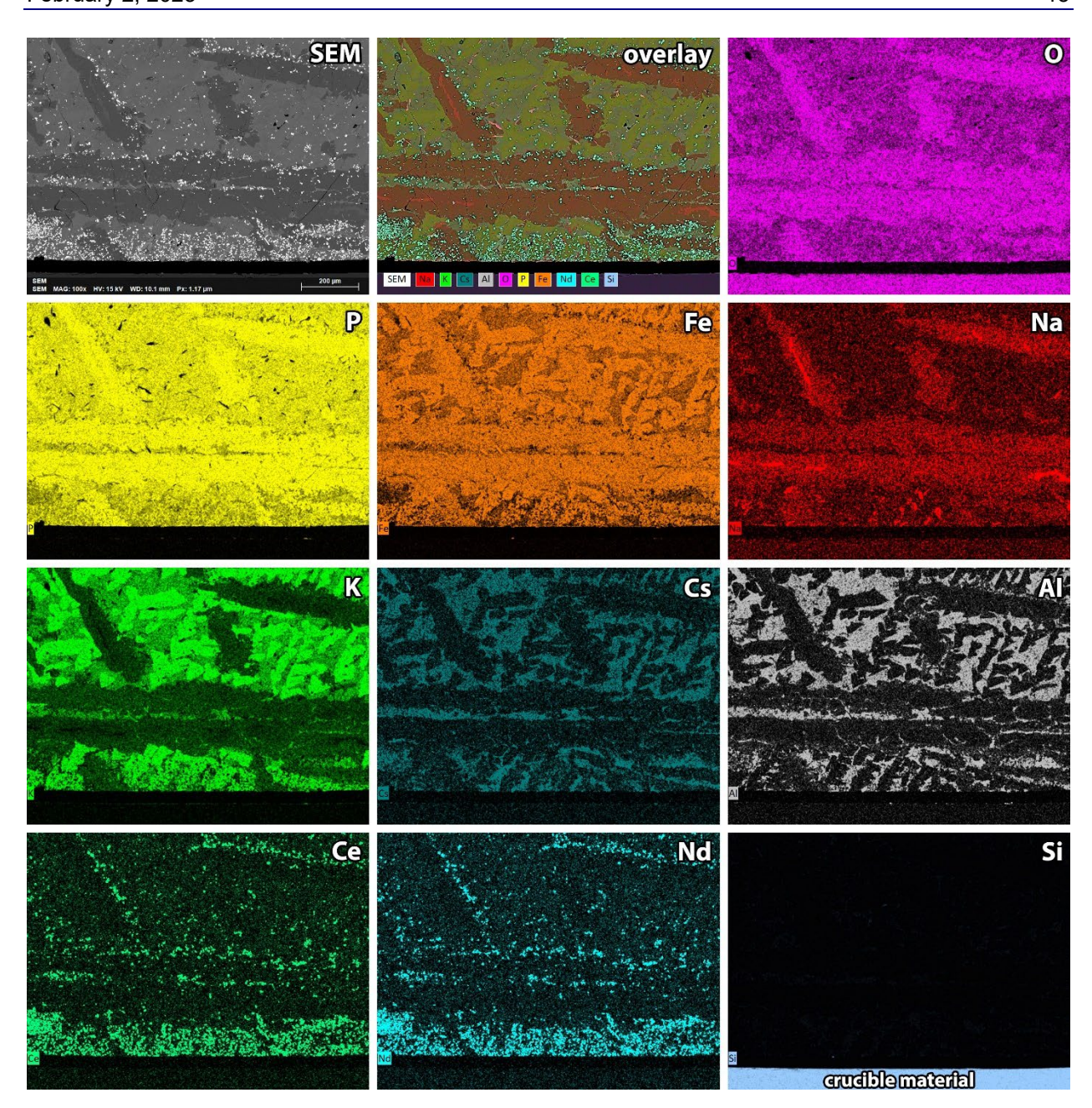


Figure 12. SEM-EDS dot map data for the CCC-treated sample run in the fused quartz crucible (see Figure 7a,c), which can be seen at the bottom of the map with an air gap between the sample and the crucible in Figure 10e,f, which is also the location in the sample where this map was collected.

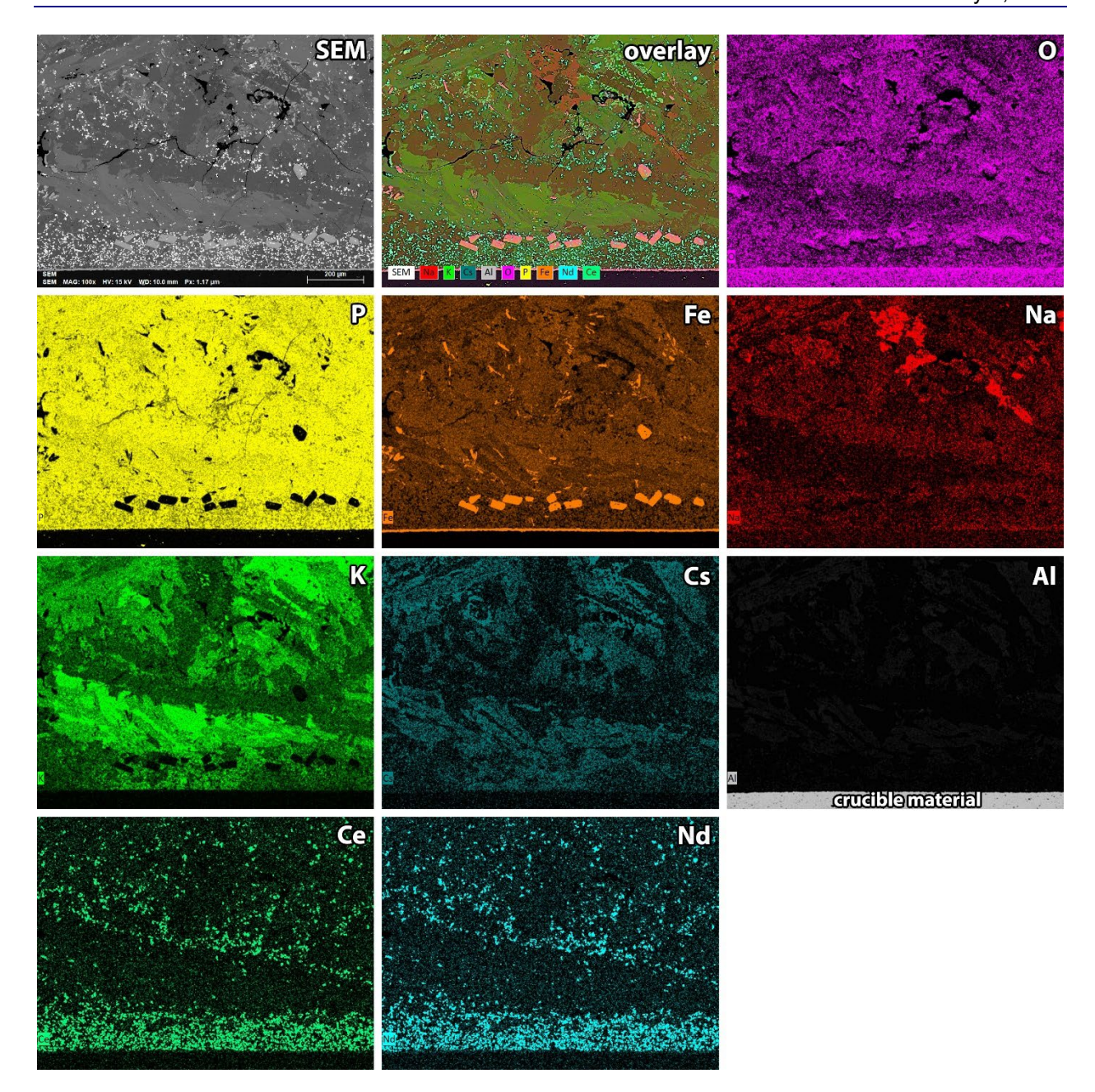


Figure 13. SEM-EDS dot map data for the CCC-treated sample run in the alumina crucible (see Figure 7b,d); the bottom of the sample is seen in the Al dot map where the crucible-sample interface can be observed. The location of this region is at the bottom of the samples (see Figure 11e,f).

Spot analyses were performed with SEM-EDS on both the CCC samples run in fused quartz and alumina crucibles and these data are provided in Figure 14 and Figure 15, respectively. The SEM micrographs in each Figure 14 and Figure 15 show the void spaces present in the samples, which could be due to thermal expansion mismatches between the compositionally different phases. Each sample contains five distinct phases that include (1) void spaces/cracks, (2) – (4) three separate gray phases varying in composition, and (5) monazite (brightest phases based on the high atomic number).

The gray phases shown in Figure 14 show very similar compositions with fluctuations in constituents where the light gray phase is high in Al, Cs, and Si while being lower in K, Fe, and Na than the other graph phases. The medium gray phase is highest in K and Fe compared to the other graph phases. The darkest gray phase is also higher in Fe and Na, but lower in P, K, Al, and Si. The monazite phase contains Ce, Nd, and P.

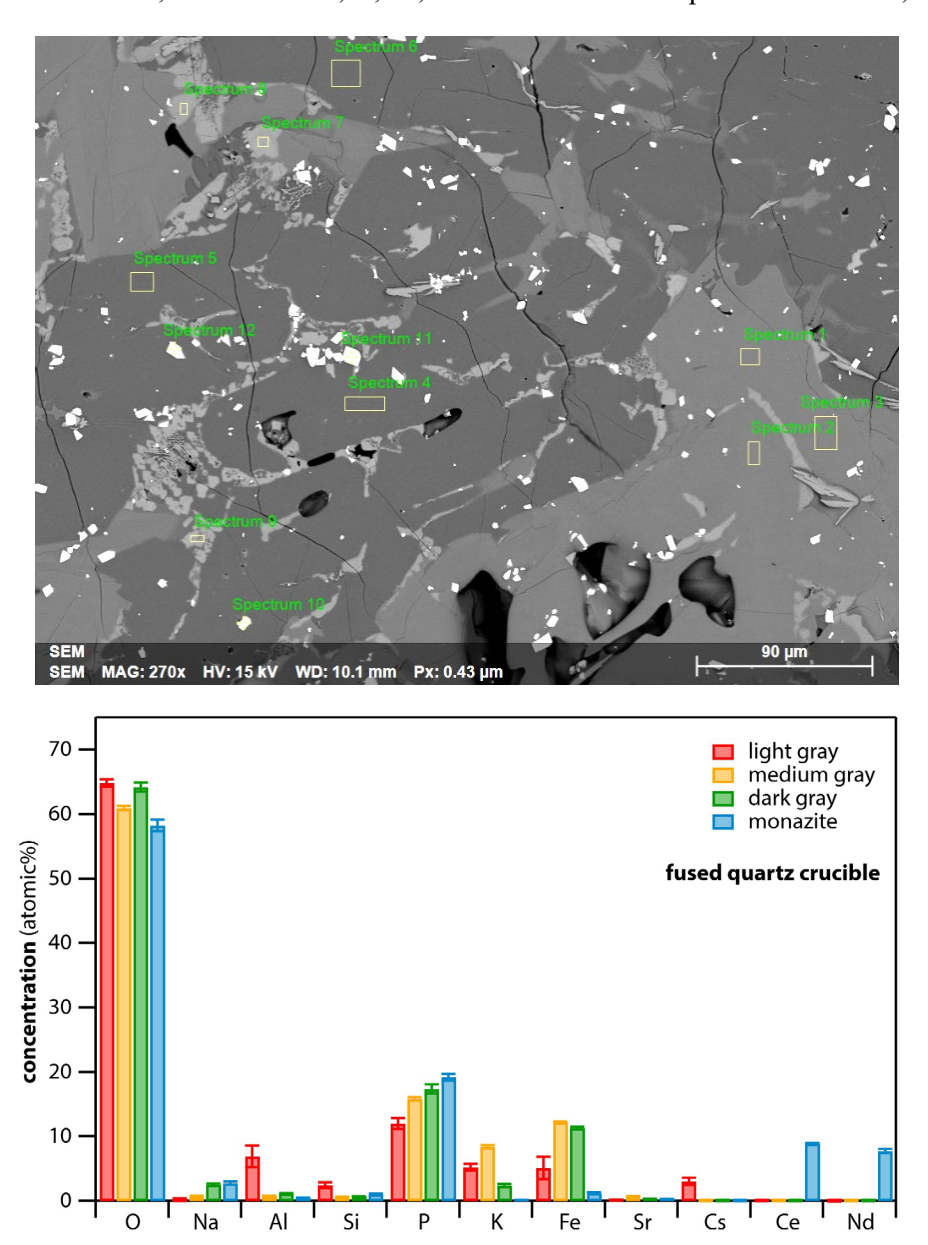


Figure 14. (top) SEM-EDS spot locations for the CCC-treated sample run in the fused quartz crucible. This region was in the middle of the sample (see Figure 10d). (bottom) EDS spot analysis from regions shown in the top figure from regions that are light gray (spots 7-9), medium gray (spots 1-3), dark gray (spots 4-6), and monazite (spots 10-12). The full dataset is found in Table A1 in Appendix A.

The light gray phase in Figure 15 is Fe_2O_3 . The medium and dark gray phases show similar compositions with fluctuations in Na, Al, K, and Sr with the balance being P and O. The monazite phase contains Ce, Nd, and P.

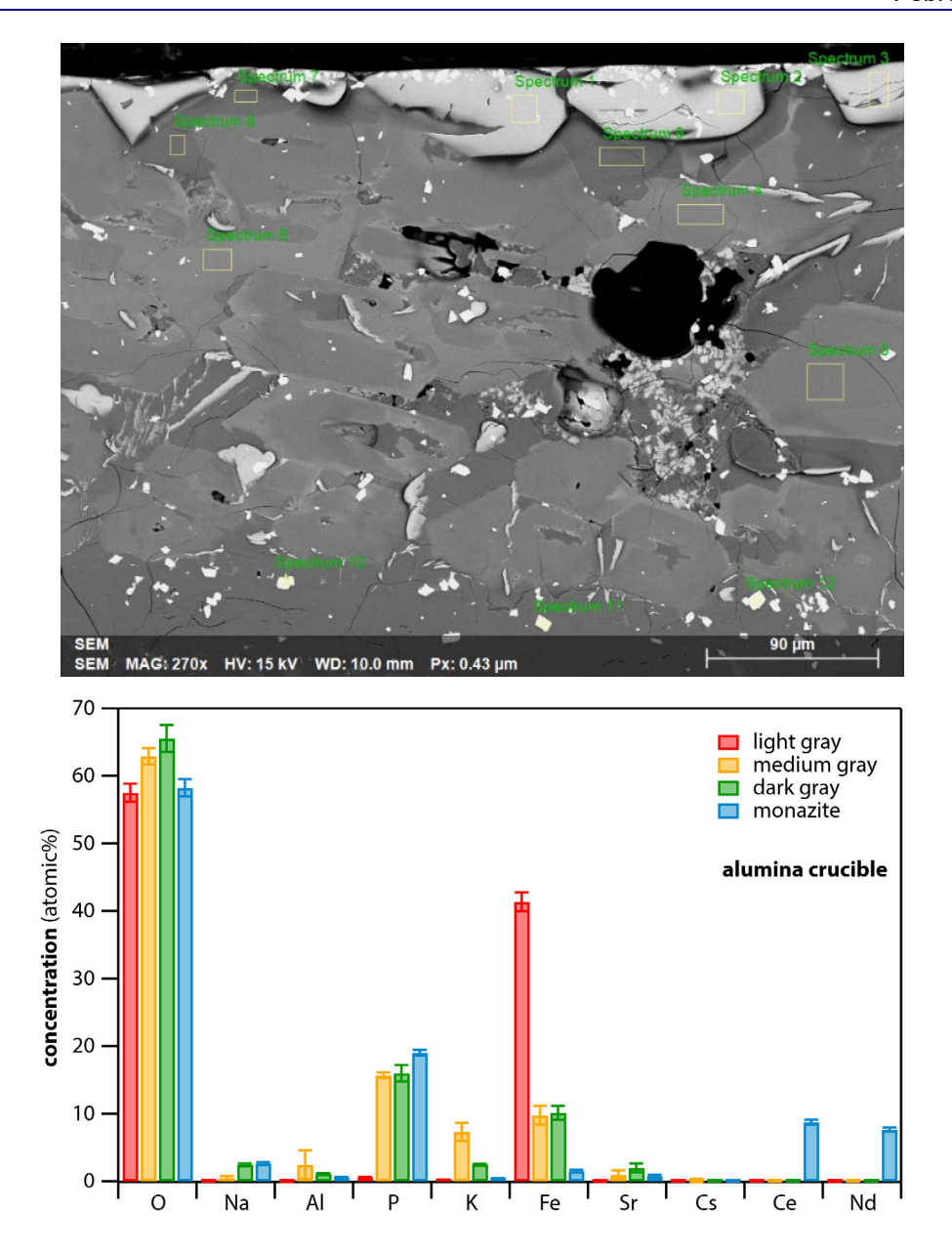


Figure 15. (top) SEM-EDS spot locations for the CCC-treated sample run in the alumina crucible. This region was at the top of the sample (see Figure 11b). (bottom) EDS spot analysis from regions shown in the top figure from regions that are light gray (spots 1-3), medium gray (spots 4-6), dark gray (spots 7-9), and monazite (spots 10-12) were the values are averages across the spots along with error bars representing standard deviations ($\pm 1\sigma$). The full dataset is found in Table A2 in Appendix A.

4.0 Summary and Conclusions

In summary, the dechlorination efficiency was ~92 mass% based on the percentage of expected NH₄Cl production and the glass was homogeneous in appearance with a shiny surface layer attributed to both phase separation and a small quantity of crystalline material [likely Li₃Fe₂(PO₄)₃ based on ICDD peak fits]. The CCC tests were run for DPF5-336 in duplicate in fused quartz and alumina crucibles. One sample each run in fused quartz and alumina crucibles were cross sectioned and analyzed with imaging, SEM-EDS, and XRD. The other duplicates were shipped to ANL for chemical durability testing. The crystalline phases, elemental distributions, and microstructures varied between the two samples with the exception of both samples containing a large fraction of monazite [i.e., (Nd,Ce)PO₄]. The results from this study were similar in many ways to the DPF5 dataset (Riley and Chong 2020). In both studies, the number of crystalline diffraction peaks far surpassed the number that allows for accurate phase identification and quantification, which was why simpler studies involving only 3 components (i.e., $P_2O_5 + Fe_2O_3 + a$ single salt additive) were pursued (Riley and Chong 2022b) after the initial DPF5 CCC study (Riley and Chong 2020). More work is needed to fully understand the effects of microstructure on the slow cooling processes within these materials, how the different components effect these processes (i.e., Li distribution has not yet been studied in these due to EDS limitations), and how some of these different phases present in CCC-treated materials effect other properties like chemical durability of the overall bulk waste form.

5.0 Acknowledgements

The authors acknowledge support on this work from John Vienna (PNNL), William Ebert and Sarah Stariha (ANL), Steve Frank, Steve Herrmann, Ken Marsden, Morgan Kropp, and Kevin Tolman (INL), Krista Carlson (University of Nevada Reno), Michael Simpson (University of Utah), Professor Richard Brow (Missouri University of Science and Technology), CW Kim (MoSci Corporation), and Ming Tang (Clemson University). Authors also acknowledge support on the DOE-NE Material Recovery and Waste Form Campaign from Ken Marsden (INL), Kimberly Gray (DOE-NE), James Willit (DOE-NE), and Stephen Kung (DOE-NE). The university collaborations were performed through the Nuclear Energy University Partnership (NEUP) Program under DOE-NE.

6.0 References

Ebert WL. 2022. Conceptual Iron Phosphate Waste Form Degradation Model. ANL/CFCT-22/48. Argonne National Laboratory, Lemont, Illinois.

Ebert WL, BJ Riley, and SM Frank. 2017. *Test Plan for Salt Treatment and Waste Form Development*. NTRD-MRWFD-2017-000191, Argonne National Laboratory, Lemont, Illinois.

Ebert WL, JA Fortner. 2019a. Analysis of Iron Phosphate Glasses for Dehalogenated Salt Waste. ANL/CFCT-19/5, Argonne National Laboratory, Lemont, Illinois.

Ebert WL, JA Fortner. 2019b. Corrosion Tests with Developmental Iron Phosphate Glass Waste Forms. ANL/CFCT-19/7, Argonne National Laboratory, Lemont, Illinois.

Riley BJ, S Chong, C Lonergan, C Skidmore. Personal communication. 2019. *Completion of Milestone M4FT-19PN030105073 – Send glasses to ANL for durability testing (PNNL-ANL)*. Pacific Northwest National Laboratory, Richland, Washington.

Riley BJ. 2020. "Electrochemical salt wasteform development: A review of salt treatment and immobilization options," *Industrial & Engineering Chemistry Research* **59**(21):9760-74.

Riley BJ, JA Peterson, JD Vienna, WL Ebert, and SM Frank. 2020. "Dehalogenation of electrochemical processing salt simulants with ammonium phosphates and immobilization of salt cations in an iron phosphate glass waste form," *Journal of Nuclear Materials* **529**:151949.

Riley BJ, S Chong. 2020. Completion of Milestone M4FT-20PN030105031: Evaluate physical properties of CCC-cooled phosphate glass waste forms. PNNL-SA-155636, Pacific Northwest National Laboratory, Richland, Washington.

Riley BJ, S Chong, CE Lonergan. 2021. "Dechlorination apparatus for treating chloride salt wastes: System evaluation and scale-up," *ACS Omega* **6**(47):32239-32252.

Riley BJ, S Chong. 2022a. Completion of Milestone M3FT-22PN030104041: Ship iron phosphate glass to ANL for chemical durability testing." PNNL-SA-173625, Pacific Northwest National Laboratory, Richland, Washington.

Riley BJ, S Chong. 2022b. "Effects of composition and canister centerline cooling on microstructure, phase distribution, and chemical durability of dehalogenated iron phosphate waste forms," *Journal of Non-Crystalline Solids* **579**:121319.

Riley BJ, S Chong, M Peterson, ET Nienhuis. 2023. *Aluminophosphate Waste Forms for Immobilizing Cations from Electrochemical Salt Wastes*. PNNL-33906, Pacific Northwest National Laboratory, Richland, Washington.

Stariha S, WL Ebert. 2020. Corrosion Behavior of Developmental Iron Phosphate Waste Forms: FY20 Status Report. ANL/CFCT-20/34, Argonne National Laboratory, Lemont, Illinois.

Stariha S, WL Ebert. 2021. Corrosion Behavior of Developmental Iron Phosphate Waste Forms: FY21 Status Report. ANL/CFCT-21/14, Argonne National Laboratory, Lemont, Illinois.

Stariha S, WL Ebert. 2022. Corrosion Behavior of Fast-Cooled Iron Phosphate Reference Material. ANL/CFCT-22/49, Argonne National Laboratory, Lemont, Illinois.

Appendix A

SEM-EDS Data

A-1. EDS Data for CCC Sample Run in a Fused Quartz Crucible

Table A1. Summary of EDS data (in atomic%) for CCC sample run in the fused quartz crucible where spectra 1-3 are the medium gray phase, spectra 4-6 are the dark gray phase, spectra 7-9 are the light gray phase, and spectra 10-12 are the monazite phase. Below each set of triplicates are average (ave) and standard deviation (SD; $\pm 1\sigma$) values for those datasets. The appearances of these locations in the sample along with the plotted data are found in Figure 14.

Spec	О	Na	Al	Si	P	K	Fe	Sr	Cs	Ce	Nd
#1	60.67	0.39	0.80	0.66	15.96	8.52	12.33	0.64	0.00	0.00	0.03
#2	60.82	0.80	0.86	0.54	15.98	8.09	12.07	0.78	0.00	0.02	0.04
#3	61.35	0.67	0.67	0.53	15.51	8.54	12.20	0.51	0.02	0.00	0.00
ave	60.95	0.62	0.78	0.58	15.82	8.38	12.20	0.64	0.01	0.01	0.02
SD	0.35	0.21	0.10	0.07	0.26	0.25	0.13	0.14	0.01	0.01	0.02
#4	63.63	2.36	1.04	0.70	18.05	2.68	11.16	0.34	0.01	0.02	0.01
#5	63.97	2.73	1.23	0.70	17.42	2.34	11.25	0.35	0.00	0.00	0.02
#6	65.00	2.48	1.16	0.71	16.62	2.18	11.54	0.31	0.00	0.00	0.01
ave	64.20	2.52	1.14	0.70	17.36	2.40	11.31	0.33	0.00	0.01	0.01
SD	0.71	0.19	0.10	0.01	0.72	0.26	0.20	0.02	0.00	0.01	0.01
#7	64.64	0.37	7.79	2.55	12.08	4.84	4.26	0.06	3.40	0.00	0.01
#8	65.48	0.03	7.93	2.84	11.20	5.09	3.93	0.06	3.43	0.00	0.00
#9	64.42	0.21	5.00	1.98	12.87	5.86	7.05	0.19	2.36	0.00	0.07
ave	64.85	0.20	6.91	2.46	12.05	5.26	5.08	0.10	3.06	0.00	0.03
SD	0.56	0.17	1.65	0.44	0.84	0.53	1.71	0.08	0.61	0.00	0.04
#10	57.94	2.46	0.55	1.07	19.38	0.18	1.36	0.31	0.00	8.85	7.90
#11	57.50	2.83	0.47	1.15	19.54	0.16	1.18	0.21	0.03	9.03	7.91
#12	59.27	2.99	0.43	0.88	18.59	0.13	1.21	0.18	0.00	8.93	7.38
ave	58.24	2.76	0.48	1.03	19.17	0.16	1.25	0.23	0.01	8.94	7.73
SD	0.92	0.27	0.06	0.14	0.51	0.03	0.10	0.07	0.02	0.09	0.30

A-2. EDS Data for CCC Sample Run in an Alumina Crucible

Table A2. Summary of EDS data (in atomic%) for CCC sample run in the alumina crucible where spectra 1-3 are the light gray phase, spectra 4-6 are the medium gray phase, spectra 7-9 are the dark gray phase, and spectra 10-12 are the monazite phase. Below each set of triplicates are average (ave) and standard deviation (SD; $\pm 1\sigma$) values for those datasets. The appearances of these locations in the sample along with the plotted data are found in Figure 15.

Spec	0	Na	Al	P	K	Fe	Sr	Cs	Ce	Nd
#1	58.97	0.00	0.07	0.65	0.21	39.92	0.03	0.02	0.06	0.09
#2	57.50	0.00	0.02	0.62	0.15	41.62	0.02	0.01	0.01	0.06
#3	56.27	0.00	0.00	0.69	0.23	42.69	0.11	0.00	0.02	0.00
ave	57.58	0.00	0.03	0.65	0.19	41.41	0.05	0.01	0.03	0.05
SD	1.35	0.00	0.03	0.04	0.04	1.40	0.05	0.01	0.02	0.04
#4	62.72	0.67	1.26	15.31	8.29	10.82	0.85	0.04	0.02	0.01
#5	64.27	0.14	4.95	15.68	5.81	8.23	0.41	0.49	0.03	0.00
#6	61.87	0.71	1.22	16.16	7.88	10.40	1.72	0.00	0.01	0.03
ave	62.96	0.50	2.48	15.72	7.32	9.81	0.99	0.18	0.02	0.01
SD	1.22	0.32	2.14	0.43	1.33	1.39	0.67	0.27	0.01	0.01
#7	67.83	2.68	1.19	14.88	2.51	9.06	1.79	0.03	0.02	0.01
#8	64.62	2.44	1.24	17.27	2.55	10.38	1.50	0.00	0.00	0.00
#9	64.24	2.33	1.07	15.94	2.63	11.04	2.73	0.02	0.00	0.00
ave	65.56	2.48	1.17	16.03	2.56	10.16	2.01	0.02	0.01	0.00
SD	1.97	0.18	0.09	1.20	0.06	1.01	0.65	0.01	0.01	0.00
#10	59.63	2.76	0.70	18.56	0.49	1.33	0.70	0.00	8.44	7.38
#11	58.13	2.45	0.58	19.34	0.48	1.66	0.68	0.01	8.90	7.77
#12	57.09	2.86	0.57	19.33	0.49	1.64	1.01	0.01	9.11	7.90
ave	58.28	2.69	0.62	19.08	0.49	1.54	0.80	0.01	8.82	7.68
SD	1.28	0.21	0.07	0.45	0.00	0.18	0.19	0.00	0.34	0.27

A-3. SEM-EDS Data for G1

The data in this section is from Riley et al. (2023) and is from G1, a glass made from oxides and carbonates of the salt components instead of using chloride salts (ERV3b). This sample had the same target composition as the DPF5-336 sample in the current study.

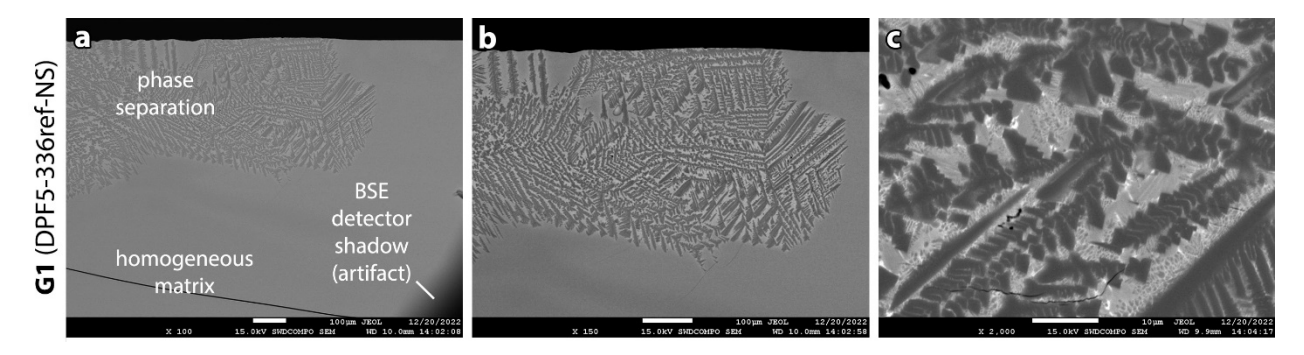


Figure A1. SEM micrographs for G1 at (a) 100×, (b) 150×, and (c) 2000× magnifications. The shadow in (a) is an artifact from the backscattered electron (BSE) detector.

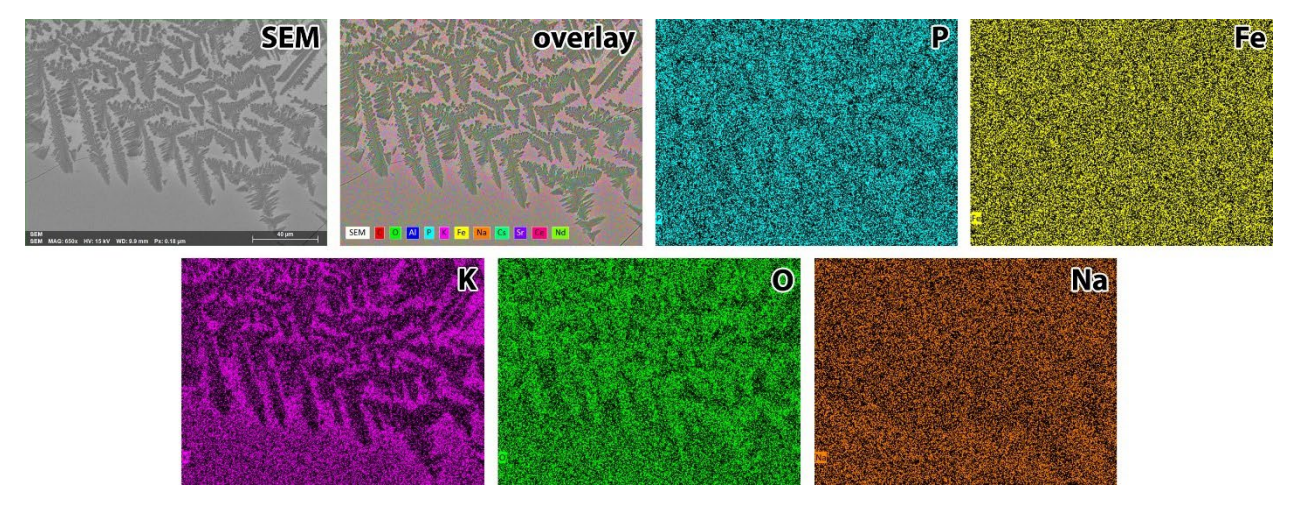


Figure A2. SEM-EDS dot map for G1 including the SEM micrograph, EDS overlay, and the elemental maps for P, Fe, K, O, and Na.

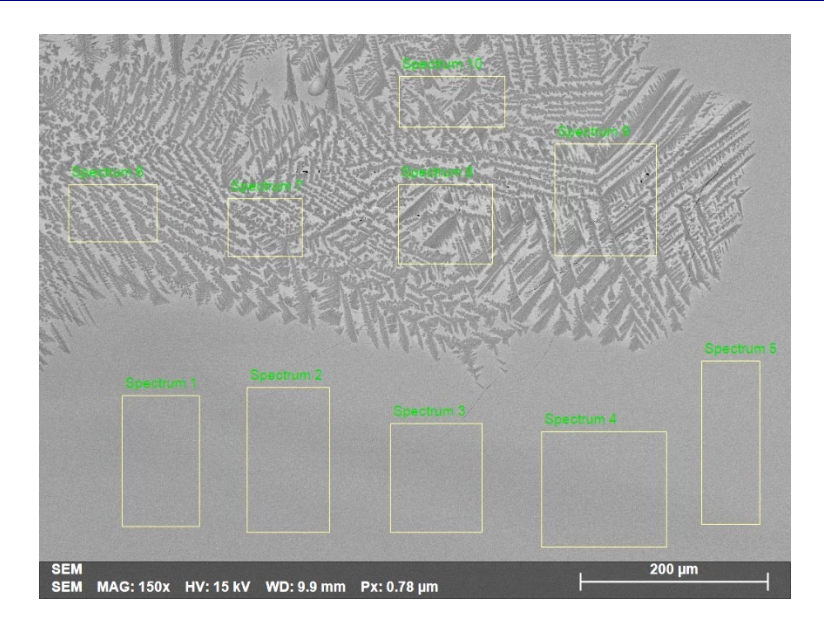


Figure A3. SEM micrograph with EDS spot analysis regions for G1 at the top of the sample where the phase separation meets the bulk matrix phase with data presented in Table A3.

Table A3. Summary of EDS spot analysis results (atomic%) from G1 (see Figure A3) including the homogeneous matrix phase (regions 1-5) and phase-separated phase (regions 6-10) as well as average (ave) and standard deviation (SD; $\pm 1\sigma$) data for like regions.

Region	О	Na	Al	P	K	Fe	Sr	Cs	Ce	Nd
reg-1	63.2	1.3	3.5	15.5	4.6	10.1	1.0	0.3	0.3	0.2
reg-2	63.1	1.3	3.4	15.6	4.5	10.1	1.1	0.3	0.4	0.2
reg-3	63.3	1.3	3.4	15.6	4.5	10.1	1.0	0.3	0.4	0.2
reg-4	63.6	1.2	3.2	15.8	4.5	9.9	1.1	0.3	0.3	0.2
reg-5	63.7	1.4	2.4	16.3	4.6	9.8	1.1	0.3	0.3	0.2
ave	63.4	1.3	3.2	15.8	4.5	10.0	1.0	0.3	0.3	0.2
SD	0.3	0.1	0.4	0.3	0.1	0.1	0.1	0.0	0.1	0.0
reg-6	63.9	1.2	2.0	16.0	4.8	10.2	1.1	0.3	0.3	0.2
reg-7	64.5	0.0	0.3	13.6	6.3	14.1	0.0	0.5	0.4	0.3
reg-8	63.6	1.4	2.0	16.2	4.6	10.4	1.0	0.2	0.4	0.2
reg-9	63.8	1.3	1.9	16.2	4.5	10.4	1.1	0.4	0.3	0.2
reg-10	64.1	1.4	2.3	15.6	4.8	9.8	1.1	0.4	0.3	0.2
ave	64.0	1.1	1.7	15.5	5.0	11.0	0.9	0.4	0.3	0.2
SD	0.4	0.6	0.8	1.1	0.7	1.8	0.5	0.1	0.1	0.0

Appendix B

Milestone Details

The details of this milestone are the following:

- Milestone Number: M4FT-23PN030104042.
- **Title**: Perform canister centerline cooling tests on DPF5-336 reference material and characterize the product.
- **Description**: Some of the DPF5-336 iron phosphate reference material being synthesized for ANL will be CCC treated and characterized. Understanding the microstructure and phase (elemental) distributions in these materials is important for understanding the performance of these waste forms in real-world melter/casting applications.
- **Due Date**: 03/31/2023
- Criteria for Completion: A memorandum will be sent to the Federal Manager, National Technical Director, and Control Account Manager summarizing this work. (*Note that a technical report also meets the qualifications of criteria for completion.*)
- Work Package: FT-23PN03010404
- Work Package Title: Off-Gas & Waste Forms PNNL
- Work Breakdown Structure: 1.02.03.01.04